Small azobenzene derivatives active against bacteria and fungi

ARTICLE *in* EUROPEAN JOURNAL OF MEDICINAL CHEMISTRY · AUGUST 2013

Impact Factor: 3.45 · DOI: 10.1016/j.ejmech.2013.07.030 · Source: PubMed

European Journal of Medicinal Chemistry 68 (2013) 178–184

Contents lists available at ScienceDirect

European Journal of Medicinal Chemistry

journal homepage: http://www.elsevier.com/locate/ejmech

Original article

Small azobenzene derivatives active against bacteria and fungi

Stefano Piotto [a], Simona Concilio [b,*], Lucia Sessa [a], Amalia Porta [a], Elena Concetta Calabrese [a], Anna Zanfardino [c], Mario Varcamonti [c], Pio Iannelli [a]

[a] Department of Pharmacy, University of Salerno, via Giovanni Paolo II, 132, 84084 Fisciano (Salerno), Italy
[b] Department of Industrial Engineering, University of Salerno, via Giovanni Paolo II, 132, 84084 Fisciano (Salerno), Italy
[c] Department of Structural and Functional Biology, University of Napoli Federico II, Via Cinthia, Complesso Monte S. Angelo, 80126 Naples, Italy

ARTICLE INFO

Article history:
Received 26 March 2013
Received in revised form
11 June 2013
Accepted 18 July 2013
Available online 11 August 2013

Keywords:
Azobenzenes
ADMET
Antimicrobial

ABSTRACT

ATP synthase and protein kinase (PKs) are prime targets for drug discovery in a variety of diseases. It is well known that numerous stilbenes are capable to interact and inhibit ATP synthase and PKs. This work focuses on a series of azobenzene based molecules having high structural similarity with antimicrobial stilbenes. An investigation was carried out analyzing the potential toxicity of a large set of molecules by means of computational analysis. A small selection of potential low toxic molecules have been therefore synthesized, characterized and finally microbiologically tested.

The synthesized compounds show potent bactericidal activity against Gram+ and a fungus, and are capable of inhibiting biofilm formation. Finally, the compounds demonstrated a thermal stability that makes them potential candidates for incorporation in polymer matrix for application as biomedical devices and food packaging.

1. Introduction

The emergence of bacterial strains resistant to the most common classes of antibiotics is prompting a dramatic quest for the development of new antimicrobial drugs.

Infections caused by resistant microorganisms often fail to respond to conventional treatment, resulting in prolonged illness and greater risk of death. According to WHO [1], about 440,000 new cases of multidrug-resistant tuberculosis (MDR-TB) emerge annually, causing at least 150,000 deaths.

A high percentage of hospital-acquired infections are caused by highly resistant bacteria, such as methicillin-resistant *Staphylococcus aureus* (MRSA).

Some stilbenes, like resveratrol, are well known natural antibiotics. Resveratrol is a phytoalexin produced in response to environmental stresses, such as wounding or pathogen attack. Resveratrol (RES) was known to possess an antimicrobial and a pronounced antifungal effect [2]. Its mechanism of action is probably the inhibition of bacterial ATP synthase and PKs [3,4]. However, a recent work of Weber [5] demonstrated that resveratrol is not effective against *Candida albicans* and other *Candida* species. Moreover, Paulo and coworkers [6] pointed out that the activity of resveratrol against Gram-positive and Gram-negative bacteria is lower than previously reported. Unfortunately, stilbenes derivatives display only moderate antimicrobial effects [7,8], and they are usually toxic compounds, a major drawback when developing new drugs.

The goal of this work was to design and synthesize molecules with similar or higher activity compared to antimicrobial stilbenes, but with reduced toxicity. Therefore we considered the azobenzenes, a class of molecules having high structural similarity with stilbenes. Though azobenzenes have been widely studied as dyers or photoresponsive materials [9–12], very little is reported about their potential antimicrobial activity. Preliminary results from molecular docking (data to be published) indicated that these compounds can inhibit ATP synthase binding at the interface between α and γ subunits of ATP synthase. Therefore, a computational investigation was carried out to study the potential toxicity of a large set of molecules. The five molecules with lowest in silico toxicity values were synthesized, chemically and thermally characterized to establish the possibility of their use in polymer matrices, and they finally underwent to microbiological tests to evaluate the antimicrobial activity and the capability to destroy biofilms.

* Corresponding author. Tel.: +39 320 7979002; fax: +39 089 964057.
E-mail address: sconcilio@unisa.it (S. Concilio).

0223-5234/$ – see front matter © 2013 Elsevier Masson SAS. All rights reserved.
http://dx.doi.org/10.1016/j.ejmech.2013.07.030

2. Results and discussion

2.1. In silico screening

We employed the in silico toxicity tool ADMET from Accelrys, to preliminarily test a series of 6156 azo compounds as listed in Table 4, Section 4.1. For each molecule we calculated the aqueous solubility [13], the blood–brain penetration after oral administration [14], the cytochrome P450 2D6 inhibition [15], and the potential liver toxicity [16]. Consistent with the literature [17–19], the vast majority of the set yielded unacceptable toxicity; only 22 molecules out of 6156 presented values of interest. The five models were calculated for the 6156 molecules and the results were plotted in Fig. 1.

In Fig. 1, the distribution of properties is evident using a multi-dimensional representation. The subset that promised less toxicity effect is indicated within a large red box. The 5 best candidates listed in Table 1 are all inside the red box. In particular, the two small cyan spheres (corresponding to **A2** and **A4** in Table 1) inside the red circle, exhibit the best overall indices. Unlike the remaining azobenzenes, that show extremely high probability of hepatotoxicity, the molecules of Table 1 have probability of being nontoxic (For interpretation of the references to color in this figure legend, the reader is referred to the web version of this article.).

Table 1
ADMET parameters of the five synthesized compounds.

Molecule	ID[a]	Solubility[b]	Hepatotoxicity	CYP2D6[c]	PSA_2D[d]	BBB[e]
A1	1144	−4.212	0.596	0.387	64.277	0.268
A2	496	−4.127	0.589	0.395	64.277	0.289
A3	820	−4.843	0.655	0.643	64.277	0.409
A4	1972	−5.001	0.655	0.712	64.277	0.439
A5	2062	−4.683	0.668	0.792	64.277	0.278

[a] Molecule identification number.
[b] Solubility is the AlogP98.
[c] Cytochrome P450 2D6 inhibition prediction.
[d] Fast polar surface area.
[e] Blood–brain barrier penetration coefficient. The values of hepatotoxicity and CYP2D6 fall in the range {0,1}. Values close to 0 correspond to low probability to cause dose-dependent toxicity against liver and cytochromes respectively. Values of BBB are the base 10 logarithm of the ratio (brain concentration)/(blood concentration).

2.2. Thermal and optical properties

The proton resonance data for **A1**–**A5** are in agreement with the expected values, as reported in Section 4.2. Thermodynamic properties of azo compounds **A1**–**A5** are given in Table 2. According to X-ray diffraction analysis **A1**–**A5**, as obtained from the synthesis, are crystalline materials, with melting temperatures ranging between 100 and 175 °C. The thermogravimetric analysis (TGA) shows that compounds **A1**, **A2**, **A3** and **A5** show initial decomposition temperatures (5% weight loss) around 200 °C. This stability indicates the possibility to incorporate the azo compounds in a large number of commercial polymers matrices that undergo high temperature melt compounding processing, in order to obtain biomedical devices and food packaging films. An exception is represented by **A4** that starts to degrade at about 84 °C. According to polarized optical microscopy, each compound shows a bright yellow or red needle crystalline habitus. From DSC analysis we studied the thermal behavior of **A1**–**A5**.

A1, **A2** and **A4** show a sharp melting peak in the first heating run and a crystallization peak in the cooling run. When heated in the second run, they show the same melting peak as in the first run. In particular, **A4** shows also a solid to solid transition in the first heating run at 110.3 °C (ΔH_{k-k} = 109.8 J/g) and, after cooling, it shows a second crystallization during the second heating run at 105.7 °C (ΔH_{c2} = 30.1 J/g), as confirmed by polarized optical microscopy observation and X-ray analysis. **A3** has a different behavior: in the first heating run it shows a solid to solid transition, confirmed by the observation at the polarized optical microscope (T_{k-k} = 151.6 °C, ΔH_{k-k} = 7.5 J/g); this is followed by the melting of this new solid form at 173.3 °C (see Table 2). In the subsequent cooling run the molecule crystallizes at 135.9 °C in a different crystalline form, which melts at 182.3 °C in the second heating run. This behavior was confirmed by X-Ray diffraction patterns. **A5** shows only the first melting peak and it is not able to crystallize from the melt; this is probably due to its asymmetric structure, which comprises a short methyl group and a longer allyl group on the same ring.

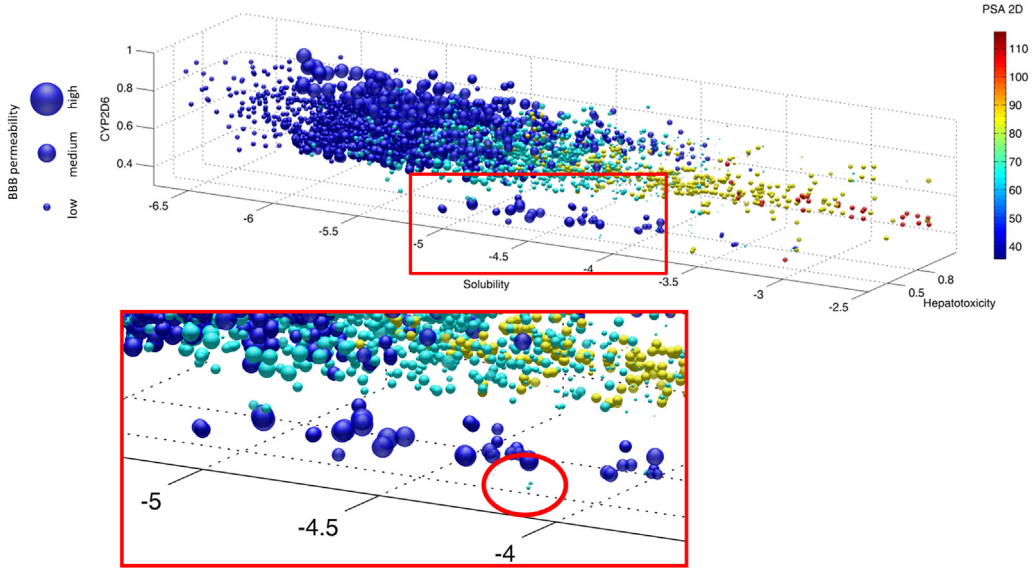

Fig. 1. 5D plot of ADMET calculation. The solubility AlogP98, the inhibition of cytochrome D6 and the hepatotoxicity are represented on the orthogonal axes. The PSA 2D is color mapped onto the spheres and the probability to cross the blood–brain barrier is indicated with the size of the spheres. The square box represents the optimal subset of the 6156 molecules of Table 1. The best candidates are indicated within the small round box.

Table 2
Optical and thermal characterization.

Molecule	Optical characterization		Thermal characterization				
	λ^{*}_{max} (nm)	ε_{max} (L mol^{-1} cm^{-1})	T_m# (°C)	$\Delta H^{\S}_m$ (J/g)	T_c# (°C)	$\Delta H^{\S}_c$ (J/g)	T_d# (°C)
A1	357	29,500	156.3	139	100.3	89.6	200.3
A2	358	30,300	151.0	112	103.6	98.3	204.9
A3	358	28,700	173.3	97.9	135.9	88.7	198.3
A4	359	30,500	174.3	110	112.6	13.7	84.9
A5	359	30,100	105.3	82.5	–	–	203.4

λ_{max} = wavelength at the principal absorption maximum, *instrument error ±0.10 nm.
ε_{max} = molar extinction coefficient at absorption maximum.
T_m = melting temperature, from DSC analysis, 10 °C/min, nitrogen flow; T_c = crystallization temperature, from DSC cooling run; T_d = temperature of 5% of weight loss in the TGA trace, 10 °C/min, nitrogen flow, #instrument error ±0.5 °C.
$\Delta H_m/\Delta H_c$ = melting/crystallization enthalpy, evaluated by integration of the peak, experimental error ±5%.

Table 3
Antimicrobial and antifungal activity.

MIC_0 (μg/mL) after 24 h					
Molecule	*S. aureus*	*L. monocytogenes*	*S. typhimurium*	*P. aeruginosa*	*C. albicans*
Resveratrol	100[a]	–	>400[a]	>400[a]	>128[b]
A1	30	50	>60	>60	30
A2	20	25	>60	>60	20
A3	20	25	>60	>60	20
A4	20	25	>60	>60	17
A5	25	>60	>60	>60	15

MIC_0: minimum inhibitory concentration required to inhibit the growth of 100% of organisms. The values are the geometric mean of at least three determinations.
[a] Data from Ref. [6].
[b] Data from Ref. [5].

The UV–vis spectra of **A1**–**A5**, in acetonitrile solution, are qualitatively independent on the number and length of flexible aliphatic segments (methyl, ethyl, allyl) attached to the azobenzene core, and only depend on the active azo-containing unit, which is the same for all compounds. The UV absorption spectra of **A1**–**A5** in trans configuration, in the 240–650 nm region, showed two bands centered around 240 and 360 nm, related respectively to the $\pi \rightarrow \pi^*$ and $n \rightarrow \pi^*$ electronic transitions of the azobenzene chromophore [9]. UV–vis data are given in Table 2.

2.3. Antimicrobial activity

The MICs (minimum inhibitory concentrations) of the **A1**–**A5** compounds for bacterial strains and *C. albicans* SC5314, determined by the microbroth dilution are shown in Table 3.

Table 3 reports the MIC_0 values along with the data on resveratrol published by Weber [5] and Paulo [6]. Compared to the reference molecule, resveratrol, all azo compounds show a higher antibacterial and antifungal activity. In particular, compounds **A4** and **A5**, exhibit MIC_0 values 4–6 times smaller than those of resveratrol.

Fig. 2 shows the effect of azo compounds (**A3**) on hyphae formation of *C. albicans*. In the absence of our compounds, an extensive hyphae formation was observed, whereas when azo compounds were present, hyphae formation was severely hampered in a concentration-dependent manner. Here, we observed a total inhibition of germination above 10 μg/mL of **A3**. The same analysis made on **A4** and **A5** is reported as Supplementary data of this article.

To determine the inhibition of biofilms formation we performed a semi-quantitative colorimetric assay that does not differentiate between live and dead cells, using different concentrations of azo compounds (8, 10, 15, 20, 25, 30, 50 and 60 μg/mL), followed by staining with CV (crystal violet). As shown in Fig. 3, *Candida* treated with different concentrations of azo compounds displayed a severe

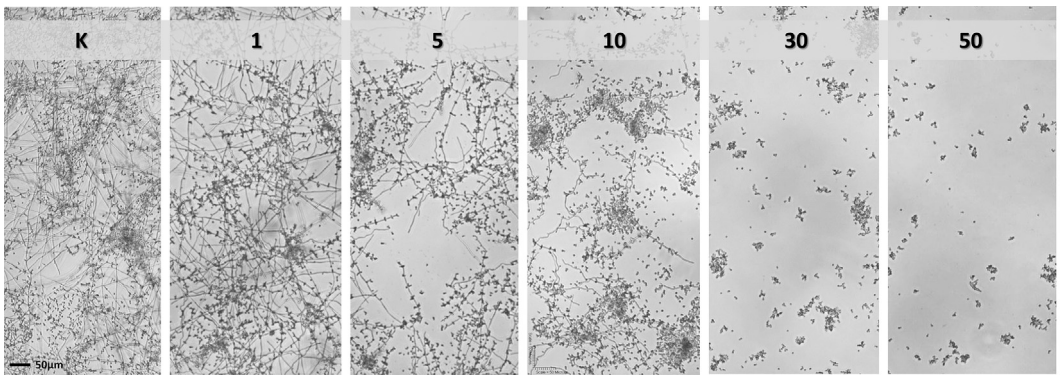

Fig. 2. Inhibition of hyphae formation in *Candida albicans* at different concentrations of A3.

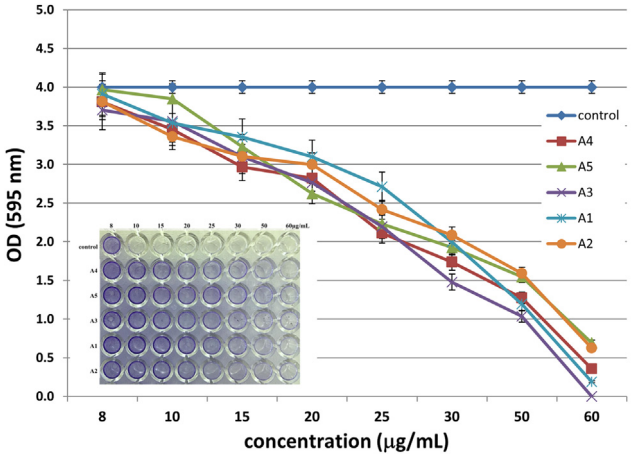

Fig. 3. Inhibition of *C. albicans* biofilm formation. Equal numbers of *Candida* cells incubated in 96-well plates for 24 h at 37 °C. Adherent cells were stained with CV.

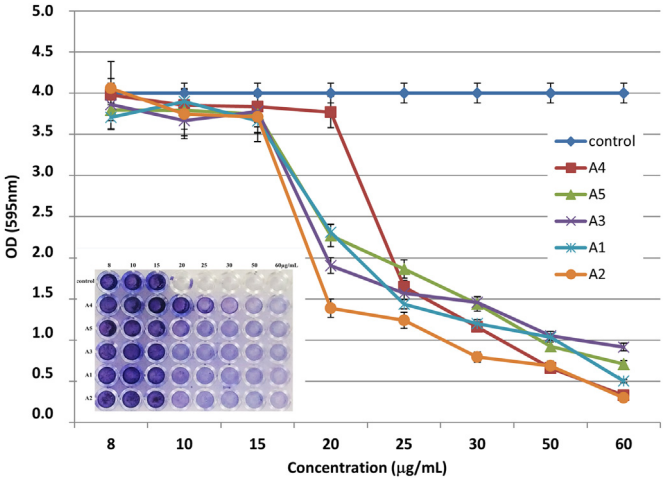

Fig. 5. Inhibition of *S. aureus* biofilm formation. *Staphylococcus* (0.2×10^7cells/mL) was incubated in 96-well plates for 24 h at 37 °C. Biofilm was stained with CV and each assay was performed 3 times.

defect in biofilm formation compared to the control. These results were confirmed by the effects of 20 µg/mL of azo compounds on *Candida* biofilms degradation using an XTT assay, which characterizes living biomass (Fig. 4).

S. aureus forms biofilms that can be detected by staining the adhered cells with CV. We analyzed the ability of different concentrations of azo compounds (8, 10, 15, 20, 25, 30, 50 and 60 µg/mL) to inhibit biofilm formation. As shown in the graph of Fig. 5, while **A4** prevents biofilms formation when used at 30 µg/mL, the other azo compounds had the same effect already at 25 µg/mL. To verify that the inhibitory effect on biofilm formation was not a result of growth inhibition, different concentrations of azo compounds (20, 25, 30 and 50 µg/mL) were added to a preformed *S. aureus* biofilm. Results in Fig. 6 confirmed that 30 µg/mL of **A1**, **A2**, **A3** and **A5** were able to degrade more than 60% of preformed biofilm. As expected, 30 µg/mL of **A4** degraded only the 40% of *S. aureus* biofilm. Complete biofilm degradation required 50 µg/mL of azo compounds.

3. Conclusions

We have designed a series of azobenzene compounds and studied their potential toxicity by means of a computational analysis. We have synthesized the molecules with the lowest in silico toxicity and studied their effects on microorganisms' cultures, representative of Gram+ and Gram− bacteria and fungi. The antimicrobial activity and the capability to destroy biofilms are promising and it indicates that these molecules may have interesting and therapeutically significant applications. In particular all azo compounds show higher antibacterial and antifungal activity than resveratrol. The preparation of polymers embedding azo-compounds is currently under investigation, since the activity of these compounds and their thermal stability suggest possible applications for food packaging and biomedical devices. Future work will include the synthesis of a larger combinatorial library of these compounds, and the test of their inhibitory effects on mammalian ATP synthase and other ATP-dependent enzymes to assess their specificity.

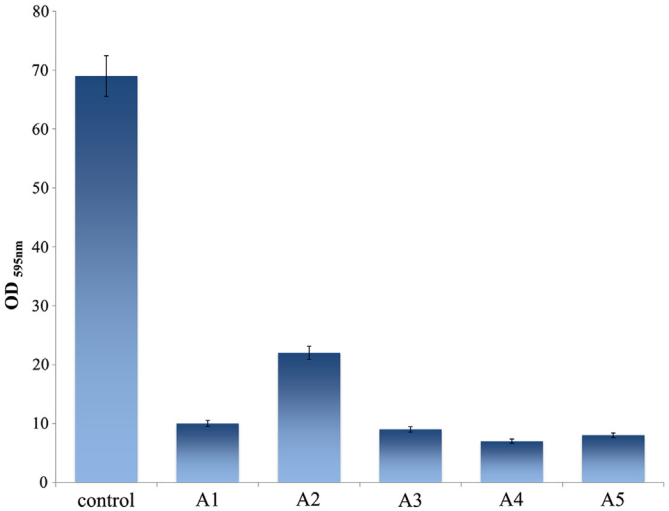

Fig. 4. XTT assay. Metabolic activity of *Candida* biofilms treated with 20 µg/mL of azo compounds, compared to control (biofilm treated with vehicle only). Each value is the mean ± S.D. of 3 independent experiments.

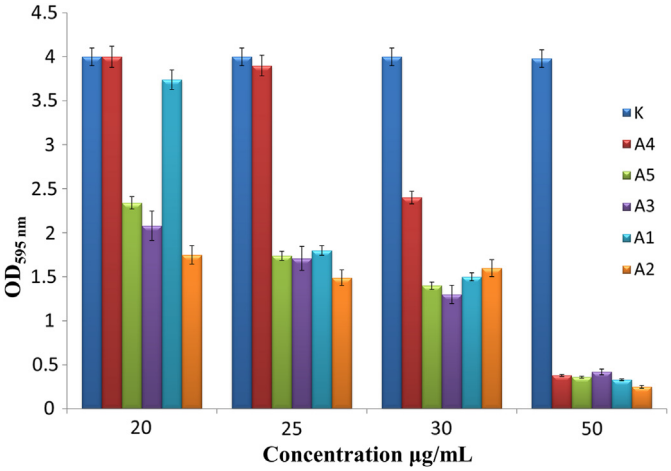

Fig. 6. *Staphylococcus* biofilm degradation. Preformed biofilms were treated for 8 h with different concentrations of azo compounds. The histogram shows the levels of treated biofilm (biofilm treated with vehicle only) as determined by CV staining. Each value is the mean ± S.D. of 3 independent experiments.

4. Experimental part

4.1. In silico screening

We have selected 18 substituents, chosen mainly for the easy of synthesis, to be linked to different positions on the subgroups AZO_A and AZO_B. The subgroup AZO_A bears three positions (R_1, R_2, and R_3) where the 18 substituents can be covalently linked. The possible combinations are $18^3 = 5832$. The subgroup AZO_B bears only two positions (R_4 and R_5) and the same set of substituents. The possible combinations are therefore $18^2 = 324$. The number of molecules that have been prepared for toxicity screening is, therefore, 6156. The 6156 considered azobenzenes are listed in Table 4.

We used the module ADMET of Discovery Studio 2.5 [20]. The aqueous solubility was estimated using the Cheng and Merz predictive model [13]. The model was generated using a dataset containing 775 compounds (molecular weight between 50 and 800). At the end of the calculation, we chose molecules with solubility levels between −5 and −3.5. The BBB (blood–brain barrier) model [14] predicts blood–brain penetration after oral administration; this model contains a quantitative linear regression model for the prediction of blood–brain penetration. The regression is based on 2D polar surface area (PSA_2D) and the solubility index AlogP98. The training set lies entirely within the 99% confidence ellipse. BBB values are the base 10 logarithm of the ratio (brain concentration)/(blood concentration). Therefore, we restricted the synthesis to the compounds with the lowest ratio. The cytochrome P450 2D6 model predicts CYP2D6 enzyme inhibition using 2D chemical structure as input [15]. The CYP2D6 score is the sum of the predicted values from all individual trees that comprise the ensemble recursive partitioning model, divided by the total number of trees in that model. Azobenzene based compounds are generally toxic, therefore we have restricted our attention to the molecules having smaller values. The computational model for predicting potential liver toxicity (HEP_TOX) of a compound was reported by Cheng and Dixon [16]; the model was developed from available literature data of 382 compounds known to exhibit liver toxicity (i.e., positive dose-dependent hepatocellular, cholestatic, neoplastic, etc.), or trigger dose-related elevated aminotransferase levels in more than 10% of human population. The model generates hepatotoxicity values in the range {0,1}, and, almost all compounds exhibit the risk of toxicity. We limited the synthesis to the compounds having the lowest HEP_TOX values.

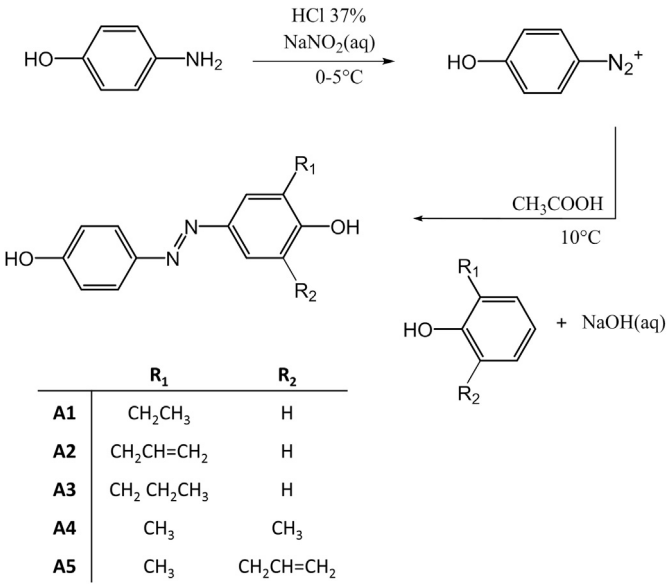

	R_1	R_2
A1	CH_2CH_3	H
A2	$CH_2CH{=}CH_2$	H
A3	$CH_2\ CH_2CH_3$	H
A4	CH_3	CH_3
A5	CH_3	$CH_2CH{=}CH_2$

Fig. 7. Synthesis scheme of azo compounds **A1**–**A5**.

4.2. Chemistry

All reagents and solvents were purchased from Sigma–Aldrich and Carlo Erba and they were used without further purification.

Table 4
Azobenzene compounds.

Base name	Scaffold	R_1, R_2, R_3, R_4, R_5	Number of molecules
AZO_A	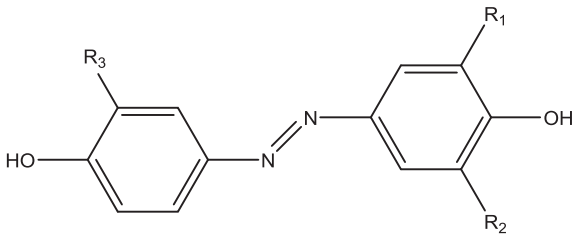	Br $CH_2CH{=}CH_2$ $CH_2CH_2CH_3$ CH_2CH_3 CH_2OH CH_2SH	5832
AZO_B	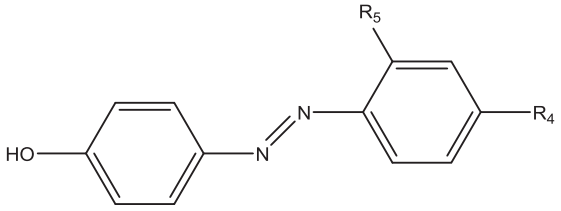	CH_3 Cl F H I $N(CH_2CH_3)_2$ $N(CH_3)_2$ NH_2 OCH_3 OH SCH_3 SH	324

A total of 6156 different azobenzene analogs have been considered for ADMET parameter prediction. Column 3 shows the substituents taken into account. For the scaffold AZO_A, three positions, R_1, R_2, and R_3, are free to change; for the scaffold AZO_B there are only two positions, R_4 and R_5, free to change.

Azo compounds **A1**–**A5** were synthesized according to the classic scheme of diazocopulation reactions, as illustrated in Fig. 7.

The procedure was the following: 2.00 g of 4-aminophenol (0.0183 mol) was suspended in a solution containing 16 mL of water and 4 mL of HCl 37% (w/w). The solution was cooled at 0–5 °C in a water–ice bath. A solution of 1.39 g of sodium nitrite (0.0202 mol) dissolved in 4 mL of water was added drop-wise, obtaining a suspension of the diazonium salt (solution A). Separately, a solution containing 1.68 g of NaOH (0.0420 mol) in 16 mL of water with 0.0183 mol of the proper phenol (depending on **A1**–**A5**) was prepared (solution B). Solution A was added drop-wise to solution B, under stirring at 12 °C. The system was left reacting for 20 min. Then the final solution was slowly added to 40 mL of an acid solution (50 mL of water and 4 mL of acetic acid), and then stirred for 30 min at 15 °C. A dark red precipitate of the azo compound formed. The crude precipitate was filtered and dried under vacuum. Yields ranged between 30 and 40%.

4.2.1. 4′-Hydroxy-(4-hydroxy-3-ethyl)-azobenzene (*A1*)

The synthesis of compound **A1** has been already reported in Ref. [21]. 4-Aminophenol and 2-ethylphenol were used as starting reagents. ^{1}H NMR (acetone-d_6): δ (ppm) = 7.77 (d, 2H); 7.61 (s, 1H); 7.58 (m, 1H); 6.95 (d, 2H); 6.93 (m, 1H); 2.64 (m, 2H); 1.20 (t, 3H).

4.2.2. 4′-Hydroxy-(4-hydroxy-3-allyl)-azobenzene (*A2*)

4-Aminophenol and 2-allylphenol were used as starting reagents. The crude product was extracted and crystallized from boiling *n*-octane (500 mL) and dried. Final crystallization from water/ethanol (10:1) gave pure **A2** as red-orange crystalline material. ^{1}H NMR (acetone-d_6): δ (ppm) = 7.78 (m, 2H); 7.71 (s, 1H); 7.64 (d, 1H); 6.99 (m, 3H); 6.07 (m, 1H); 5.07 (m, 2H); 3.47 (m, 2H).

4.2.3. 4′-Hydroxy-(4-hydroxy-3-propyl)-azobenzene (*A3*)

4-Aminophenol and 2-propylphenol were used as starting reagents. The crude product was extracted and crystallized from boiling *n*-octane (100 mL) and dried. Final crystallization from boiling water/ethanol (3:1) gave pure **A3** as gold yellow crystalline material. ^{1}H NMR (DMSO-d_6): δ (ppm) = 7.72 (d, 2H), 7.58 (d, 1H), 7.54 (d, 1H), 6.92 (d, 2H), 2.57 (m, 2H), 1.61 (m, 2H), 0.94 (t, 3H).

4.2.4. 4′-Hydroxy-(4-hydroxy-3,5-dimethyl)-azobenzene (*A4*)

4-Aminophenol and 2,6-dimethylphenol were used as starting reagents. The crude product was extracted and crystallized from boiling *n*-octane (100 mL) and dried. Final crystallization from boiling water/ethanol (3:1) gave pure **A4** as orange crystalline material. ^{1}H NMR (DMSO-d_6): δ (ppm) = 7.71 (d, 2H), 7.48 (s, 2H), 6.91 (d, 2H), 2.26 (s, 6H).

4.2.5. 4′-Hydroxy-(4-hydroxy-3-methyl-5-allyl)-azobenzene (*A5*)

4-Aminophenol and 2-allyl-6-methyphenol were used as starting reagents. The crude product was extracted and crystallized from boiling *n*-octane (100 mL) and dried. After crystallization from boiling water/ethanol (3:1), final crystallization from boiling water gave pure **A5** as red crystalline material. ^{1}H NMR (DMSO-d_6): δ (ppm) = δ 7.72 (d, 2H), 7.49 (d, 2H), 6.91 (d, 2H), 6.00 (m, 1H), 5.10 (t, J = 12.0 Hz, 2H), 2.28 (s, 3H).

4.3. Thermal characterization

Thermal measurements were performed by a DSC-7 Perkin Elmer calorimeter under nitrogen flow at 10 °C/min rate. Polarized optical microscopy was performed by a Jenapol microscope fitted with a Linkam THMS 600 hot stage. X-ray diffraction patterns on powder samples of the polymers were recorded on a flat film camera Ni-filtered Cu-Kα radiation. The Fujifilm MS 2025 imaging plate and a Fuji Bioimaging analyzer System, model BAS-1800, were used for digitizing the diffraction patterns. ^{1}H NMR spectra were recorded with a Bruker DRX/400 Spectrometer. Chemical shifts are reported relative to the residual solvent peak (acetone-d_6: H = 2.05 ppm; dimethylsulfoxide-d_6: H = 2.50 ppm). UV absorption spectra of the samples were recorded at 25 °C in acetonitrile solution, on a Perkin–Elmer Lambda 19 spectrophotometer. The spectral region 650–240 nm was investigated by using cell path length of 1 cm. Azobenzene chromophore concentration of about 3.0×10^{-5} mol L^{-1} was used.

4.4. Bacterial strains and minimum inhibitory concentrations (MICs)

The in vitro minimum inhibitory concentrations (MICs) of each compound were determined against *C. albicans* SC5314 [22] by the micro-broth dilution method in 96-well microtest plates according to the guidelines suggested by the Clinical and Laboratory Standards Institute (CLSI) [23], using three separate plates each containing the same batch of azo compounds. Microtiter plates containing 100 μL of two-fold serial dilutions of azo compounds in RPMI 1640 medium (with L-glutamine, without glucose and $NaHCO_3$, buffered to pH 7.0 with 0.165 M 4-morpholinepropanesulfonic acid [MOPS] buffer) were inoculated with 100 μL of cells containing 2.5×10^3 yeast/mL and incubated at 35 °C for 24 h. The resulting MICs were visually read as the lowest concentration of compound causing an absence of growth (optically clear) in comparison to the drug-free growth control.

For *S. aureus* A170 (kindly provided by Prof. R. Capparelli from the University of Naples, Italy), *Listeria monocytogenes* [24], *Salmonella typhimurium* [25], *Pseudomonas aeruginosa* ATCC-27853, MIC values of each compound were determined by the serial broth microdilution method as reported by Patton [26]. Therefore, flat-bottom polystyrene microtiter plates containing 100 μL of two-fold serial dilutions (six replicates per dilution) of azo compounds were inoculated with 100 μL of ~5×10^5 CFU/mL of each bacteria grown in Mueller–Hinton broth 2 (cation-adjusted MHB; Sigma–Aldrich, Milan, Italy). Control wells contained broth only (negative control) or bacteria and broth (positive control).

Plates were incubated at 37 °C with shaking at 160 rpm for 24 h. Data were analyzed according to Patton et al. [26]. Briefly, the optical density was determined just before the incubation (T_0) and again after 24 h incubation (T_{24}) at 600 nm. The OD for each replicate at T_0 was subtracted from the OD for each replicate at T_{24}. The adjusted OD of each control well was then assigned a value of 100% growth. The percent inhibition of growth was thus determined using the formula: percent inhibition = 1 − (OD test well/OD of corresponding control well) × 100. The MIC is reported as the lowest concentration of azo compounds which results in 100% inhibition of growth.

4.5. Candida morphological analysis

Hyphal growth of *Candida* treated cells was induced using RPMI 1640 medium, supplemented with 2.5% fetal calf serum, 20 mM HEPES, 2 mM L-glutamine, and 16 mM sodium hydrogen carbonate (pH 7.0, Gibco-BRL). Stationary yeast cells were inoculated into a fresh pre-warmed medium at a density of 6×10^6 cells/mL in a flat-bottom 96 well microtiter plates. Different concentrations of azo compounds (ranging from 1 to 50 μg/mL) were added to each well. After incubation at 37 °C for 24 h, each microtiter plate was examined using an inverted microscope to monitor phenotypic modification and hyphae formation.

4.6. Biofilms analysis

C. albicans cells were grown for 24 h at 28 °C in YPD broth (20 g of peptone, 10 g of yeast extract, 20 g of glucose per liter). These were washed twice with sterile PBS (10 mM phosphate buffer, 2.7 mM

potassium chloride, 137 mM sodium chloride, pH 7.4, Sigma), and re-suspended in RPMI 1640 supplemented with MOPS at 10^6 cells/mL. The cell suspension (200 μL) was seeded in pre-sterilized, polystyrene flat-bottom 96-well plates and incubated for 24 h at 37 °C. After biofilm formation, 20 μg/mL of azo compounds were added to each well and incubated 8 h at 37 °C. Afterward, the medium was aspirated, and non-adherent cells were removed by washing biofilms 3 times with 200 μL of sterile PBS. Biofilms were quantified by the 2,3-bis(2-methoxy-4-nitro-5-sulfophenyl)-2*H*-tetrazolium-5-carboxanilide (XTT) reduction assay [27]. Briefly, XTT (Sigma–Aldrich, Milan, Italy) was dissolved in PBS at a final concentration of 1 mg/mL. The solution was filter-sterilized using a 0.22 μm-pore-size filter and stored at −70 °C until required. Menadione (Sigma–Aldrich, Milan, Italy) solution (0.4 mM) was also prepared and filtered. Before each assay, XTT solution was thawed and mixed with menadione solution at a volume ratio of 20 ÷ 1. The XTT–menadione solution (250 μL) was then added to each well. The microtiter plates were then incubated in the dark for 1 h at 37 °C. Following incubation, 250 μL of the XTT-menadione solution was recovered and centrifuged (to eliminate interference of cells with colorimetric readings); 100 μL of the solution was transferred to new wells, and the color change resulting from XTT reduction was measured at 490 nm with a microtiter plate reader (LAB system multiscan EX). Each assay was performed 3 times.

A similar protocol has been used for the inhibition of *Candida* biofilm by the azo compounds [28]. Briefly, following the adhesion phase of 100 μL of 2×10^6 cells/mL of *C. albicans* on flat-bottom polystyrene microtiter plates, wells were washed twice with 150 μL of PBS to remove loosely adherent cells. The biofilms were allowed to develop up to 24 h at 37 °C in the presence of different concentrations of azo compounds (ranging from 8 to 60 μg/mL). For the photographs, non-adherent cells were removed by washing, and adherent cells were stained with crystal violet (CV) 0.3% solution. Images were captured with a Canon EOS 450d.

In order to assess the *S. aureus* biofilm formation, bacteria were grown overnight in MHB medium. Cultures were then diluted to approximately 10^7 CFU/mL in fresh MHB medium, and 200 μL was used to inoculate flat-bottom 96-well polystyrene microtiter plates containing different concentrations of azo compounds (from 8 to 60 μg/mL). After incubation for 24 h at 37 °C without shaking, the plate wells were washed twice with phosphate-buffered saline (pH 7.2) to remove non-adherent bacteria and dried in an inverted position. Finally, the adherent cells were stained with CV 0.3%.

Images were acquired using a Canon EOS 450d and processed with Microsoft Office 2010.

Similarly, *S. aureus* (200 μL of 10^4 to 10^5 CFU/mL) was inoculated in microtiter plate and incubated for 18–24 h at 35 °C to allow biofilm formation. Afterward, serial diluted solutions of azo compounds (20, 25, 30 and 50 μg/mL) were added on each well and incubated 8 h at 37 °C. For crystal violet staining, wells were rinsed with water to remove loosely adherent cells and then stained for 1 min with 200 μL of Gram's crystal violet. Wells were rinsed with water and dried. The amount of biofilm mass was obtained by destaining the wells with 200 μL of 33% acetic acid and then measuring the absorbance of the CV solution in a microplate spectrophotometer set at 595 nm.

Appendix A. Supplementary data

Supplementary data associated with this article can be found in the online version, at http://dx.doi.org/10.1016/j.ejmech.2013.07.030.

References

[1] WHO. Available from: http://www.who.int/mediacentre/factsheets/fs194/en/.

[2] H.J. Jung, Y. Seu, D. Lee, Candicidal action of resveratrol isolated from grapes on human pathogenic yeast *C. albicans*, Journal of Microbiology and Biotechnology 17 (2007) 1324.

[3] P.K. Dadi, M. Ahmad, Z. Ahmad, Inhibition of ATPase activity of *Escherichia coli* ATP synthase by polyphenols, International Journal of Biological Macromolecules 45 (2009) 72–79.

[4] N. Chinnam, P.K. Dadi, S.A. Sabri, M. Ahmad, M.A. Kabir, Z. Ahmad, Dietary bioflavonoids inhibit *Escherichia coli* ATP synthase in a differential manner, International Journal of Biological Macromolecules 46 (2010) 478–486.

[5] K. Weber, B. Schulz, M. Ruhnke, Resveratrol and its antifungal activity against *Candida* species, Mycoses 54 (2011) 30–33.

[6] L. Paulo, S. Ferreira, E. Gallardo, J.A. Queiroz, F. Domingues, Antimicrobial activity and effects of resveratrol on human pathogenic bacteria, World Journal of Microbiology and Biotechnology 26 (2010) 1533–1538.

[7] Z. Ahmad, M. Ahmad, F. Okafor, J. Jones, A. Abunameh, R.P. Cheniya, I.O. Kady, Effect of structural modulation of polyphenolic compounds on the inhibition of *Escherichia coli* ATP synthase, International Journal of Biological Macromolecules 50 (2012) 476–486.

[8] S. Albert, R. Horbach, H.B. Deising, B. Siewert, R. Csuk, Synthesis and antimicrobial activity of (E) stilbene derivatives, Bioorganic & Medicinal Chemistry 19 (2011) 5155–5166.

[9] D. Acierno, E. Amendola, V. Bugatti, S. Concilio, L. Giorgini, P. Iannelli, S.P. Piotto, Synthesis and characterization of segmented liquid crystalline polymers with the azo group in the main chain, Macromolecules 37 (2004) 6418–6423.

[10] S. Concilio, V. Bugatti, P. Iannelli, S. Piotto, Synthesis and characterization of new photoluminescent oxadiazole/carbazole-containing polymers, International Journal of Polymer Science 2010 (2010) 1–6.

[11] D. Attianese, M. Petrosino, P. Vacca, S. Concilio, P. Iannelli, A. Rubino, S. Bellone, Switching device based on a thin film of an azo-containing polymer for application in memory cells, Electron Device Letters, IEEE 29 (2008) 44–46.

[12] L. Angiolini, L. Giorgini, F. Mauriello, P. Rochon, Optically active methacrylic copolymers with side-chain azoaromatic and 9-phenylcarbazole moieties, Reactive and Functional Polymers 72 (2012) 1–10.

[13] A. Cheng, K.M. Merz, Prediction of aqueous solubility of a diverse set of compounds using quantitative structure–property relationships, Journal of Medicinal Chemistry 46 (2003) 3572–3580.

[14] W.J. Egan, G. Lauri, Prediction of intestinal permeability, Advanced Drug Delivery Reviews 54 (2002) 273–289.

[15] R.G. Susnow, S.L. Dixon, Use of robust classification techniques for the prediction of human cytochrome P450 2D6 inhibition, Journal of Chemical Information and Computer Sciences 43 (2003) 1308–1315.

[16] A. Cheng, S.L. Dixon, In silico models for the prediction of dose-dependent human hepatotoxicity, Journal of Computer-Aided Materials Design 17 (2003) 811–823.

[17] M.A. Brown, S.C. De Vito, Predicting azo dye toxicity, Critical Reviews in Environmental Science and Technology 23 (1993) 249–324.

[18] H. Mori, Y. Mori, S. Sugie, N. Yoshimi, M. Takahashi, H. Ni-i, H. Yamazaki, K. Toyoshi, G.M. Williams, Genotoxicity of a variety of azobenzene and aminoazobenzene compounds in the hepatocyte/DNA repair test and the Salmonella/mutagenicity test, Cancer Research 46 (1986) 1654–1658.

[19] H. Takahashi, T. Ishioka, Y. Koiso, M. Sodeoka, Y. Hashimoto, Anti-androgenic activity of substituted azo-and azoxy-benzene derivatives, Biological and Pharmaceutical Bulletin 23 (2000) 1387–1390.

[20] Accelrys, Discovery Studio 2.5. Available from: http://accelrys.com/products/discovery-studio/.

[21] S. Piotto, S. Concilio, L. Sessa, P. Iannelli, A. Porta, E.C. Calabrese, M.R. Galdiand, L. Incarnato, Novel antimicrobial polymer films active against bacteria and fungi, Polymer Composites (2013), http://dx.doi.org/10.1002/pc.22410.

[22] E.C. Calabrese, S. Castellano, M. Santoriello, C. Sgherri, M.F. Quartacci, L. Calucci, A.G. Warrilow, D.C. Lamb, S.L. Kelly, C. Milite, I. Granata, G. Sbardella, G. Stefancich, B. Maresca, A. Porta, Antifungal activity of azole compounds CPA18 and CPA109 against azole-susceptible and -resistant strains of Candida albicans, Journal of Antimicrobial Chemotherapy (2013).

[23] CLSI, Reference Method for Broth Dilution Antifungal Susceptibility Testing of Yeasts; Approved Standard – Third Edition, Clinical and Laboratory Standards Institute CLSI, Wayne, PA, 2008.

[24] S. Sayem, E. Manzo, L. Ciavatta, A. Tramice, A. Cordone, A. Zanfardino, M. De Felice, M. Varcamonti, Anti-biofilm activity of an exopolysaccharide from a sponge-associated strain of *Bacillus licheniformis*, Microbial Cell Factories 10 (2011) 74.

[25] A. Porta, Z. Török, I. Horvath, S. Franceschelli, L. Vígh, B. Maresca, Genetic modification of the Salmonella membrane physical state alters the pattern of heat shock response, Journal of Bacteriology 192 (2010) 1988–1998.

[26] T. Patton, J. Barrett, J. Brennan, N. Moran, Use of a spectrophotometric bioassay for determination of microbial sensitivity to manuka honey, Journal of Microbiological Methods 64 (2006) 84–95.

[27] W. da Silva, J. Seneviratne, N. Parahitiyawa, E. Rosa, L. Samaranayake, A. Del Bel Cury, Improvement of XTT assay performance for studies involving *Candida albicans* biofilms, Brazilian Dental Journal 19 (2008) 364–369.

[28] Y. Jin, H. Yip, Y. Samaranayake, J. Yau, L. Samaranayake, Biofilm-forming ability of *Candida albicans* is unlikely to contribute to high levels of oral yeast carriage in cases of human immunodeficiency virus infection, Journal of Clinical Microbiology 41 (2003) 2961–2967.